Dalton Transactions

Accepted Manuscript

ROYAL SOCIETY OF CHEMISTRY

www.rsc.org/dalton

Cite this: DOI: 10.1039/c0xx00000x

www.rsc.org/xxxxxx

Full Article

Nickel(II) radical complexes of thiosemicarbazone ligands appended by salicylidene, aminophenol and aminothiophenol moieties †

Amélie Kochem,[a,b] Gisèle Gellon,[a] Olivier Jarjayes,[a] Christian Philouze,[a] Amaury du Moulinet d'Hardemare,[a] Maurice van Gastel[b] and Fabrice Thomas[a]*

Received (in XXX, XXX) Xth XXXXXXXXX 20XX, Accepted Xth XXXXXXXXX 20XX
DOI: 10.1039/b000000x

The nickel(II) complexes of three unsymmetrical thiosemicarbazone-based ligands featuring a sterically hindered salicylidene (**1**), aminophenol (**2**) or thiophenol (**3**) moiety were synthesized and structurally characterized. The metal ion lies in an almost square planar geometry in all the complexes. The cyclic voltammetry (CV) curve of **1** shows an irreversible oxidation wave at E_p^a = 0.49 V, which is assigned to the phenoxyl/phenolate redox couple. The CV curves of **2** and **3** display a reversible one-electron oxidation wave ($E_{1/2}$ = 0.26 and 0.22 V vs Fc^+/Fc, respectively) and an one-electron reduction wave ($E_{1/2}$ = -1.58 and -1.46 V, respectively). The cations $\mathbf{2}^+$ and $\mathbf{3}^+$ as well as the anions $\mathbf{2}^-$ and $\mathbf{3}^-$ were generated. The EPR spectra of the cations in THF show a rhombic signal at g_1 = 2.034, g_2 = 2.010 and g_3 = 1.992 ($\mathbf{2}^+$) and g_1 = 2.069, g_2 = 2.018, g_3 = 1.986 ($\mathbf{3}^+$) that is consistent with a main radical character of the complexes. The difference in anisotropy is assigned to the different nature of the radical, iminosemiquinonate *vs.* iminothiosemiquinonate. The anions display an isotropic EPR signal at g_{iso} = 2.003 ($\mathbf{2}^+$) and 2.006 ($\mathbf{3}^+$), which is indicative of a main α-diimine radical character of the compounds. Both the anions and cations exhibit charge transfer transitions of low to moderate intensity in their visible spectrum. Quantum chemical calculations (B3LYP) reproduce both the g-values and Vis-NIR spectra of the complexes. The radical anions readily react with dioxygen to give the radical cations. $\mathbf{2}^+$ catalyzes the aerobic oxidation of benzyl alcohol into benzaldehyde.

Introduction

The coordination chemistry of ligands bearing redox non-innocent moieties,[1] in particular phenolate groups,[2] has attracted a considerable interest during the last decade. This stems from the discovery of metal-radical entities in the active site of several metalloenzymes.[3,4] The prototypical example is Galactose oxidase (GO),[3] which harbours an active site constituted by a tyrosyl radical ($Tyr_{272}^{\bullet}$) coordinated to a copper ion. Owing to their ability to mediate electron transfers during turnovers or even break chemical bonds [4] redox non-innocent ligands can profundly affect the reactivity and enhance the catalytic efficiency of a given metal complex. This strategy has been applied to design new classes of inorganic catalysts for several chemical transformations. The most straightforward are aerobic oxidations, especially alcohol oxidations using phenoxyl-based compounds (GO mimics), [5-7] but recently [2+2]cycloadditions,[8] nitrene [9] and oxygen-transfer [10] reactions and more generally oxidative additions were reported by several groups. [11]

Symmetrical bis(thiosemicarbazones) ligands are believed to stabilize low oxidation states of many complexes, the best described being copper ones (molecule A, scheme 1). This is mostly due to their soft N_2S_2 coordination sphere that accomodates low valent copper ion. Depending on the ligand denticity, either monomeric, dimeric or hexameric copper(I) complexes were isolated (Scheme 2),[13] although alternative copper(II)-radical formulations were recently proposed for the reduced anions on the basis of DFT calculations.[14] The potentiality of thiosemicarbazones complexes to support a reversible oxidative redox chemistry has been established by electrochemistry. [12-14] The electronic structure of the oxidized state however remains highly speculative, both the Cu(III) or Cu(II)-ligand radical formulations being proposed for the cations.[14] The redox non-innocence of the thiosemicarbazone ligand has been nicely demonstrated by Keppler *et al.* on the homoleptic Ga(III) bis(thiosemicarbazone) complex depicted in scheme 1B.[15] They showed that the complex undergoes two reversible electron transfers, although the Ga(III) ion is redox-innocent. The redox non-innocence of the ligand is herein not directly imputable to the thiosemicarbazone moiety. It arises from the presence of a terminal α-diimine unit, which can be reduced into a π-radical anion. Gerbeleu *et al.* [16] and lately Wieghardt *et al.* [17] also showed that the complexes of several S-methyl-1-phenyl-isothiosemicarbazide ligands exhibit a ligand-centered redox activity. The hydrazyl anion radical character of the ligand was confirmed by X-ray crystal structures (molecule C, scheme 1). In contrast, a metal-centered redox activity was reported for the copper complex D depicted in scheme 1, which was crystallized under both its copper(II) and copper(III)

oxidation states. [18]

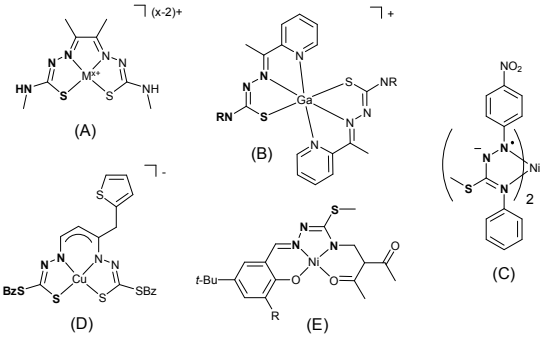

Scheme 1. Representative complexes involving thiosemicarbazone units. A) ligand or metal-centered redox processes; [12-14] B) ligand-centered reductive chemistry; [15] C) radical anion species; [16] D) metal-centered redox processes; [18] E) ligand-centered oxidative chemistry (R = *t*-Bu, SMe or SPh). [20]

A couple of years ago some thiosemicarbazone ligands appended by phenol moieties were described in the literature.[19-20] A very interesting association of a sterically hindered (and thus pro phenoxyl) phenol moiety and a thiosemicarbazone unit in a single ligand have been described recently by Arion *et al.* (molecule E, scheme 1).[20] They showed that complex E undergoes a ligand-centered oxidation process, affording a persistent phenoxyl radical species. [20] They also reported a reduction wave for E which was irreversible. This result is rather unexpected since compound C (Scheme 1), which harbours a S-methyl-thiosemicarbazide unit coordinated in a similar fashion was isolated and even crystallized under its reduced hydrazyl form.

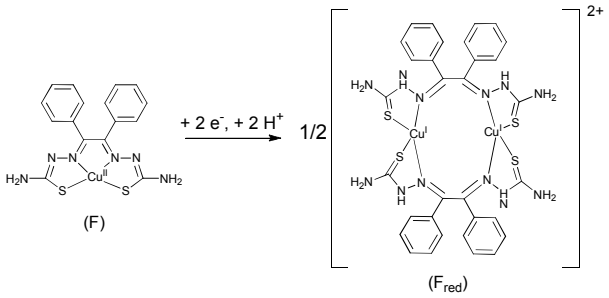

Scheme 2. Reduction of copper-thiosemicarbazone complexes. [9a]

We herein describe an unprecedented family of ligands based on a thiosemicarbazone-α-diimine backbone, which is appended by *o,p*-sterically hindered salicylidene, aminophenol or aminothiophenol moieties (Scheme 3). While the phenol-based moieties used here are the precursors of oxidatively generated radicals, we hypothesized that the thiosemicarbazone unit would stabilize efficiently a low oxidation state of the corresponding complexes. We focused in this article on the nickel complexes (**1**, **2** and **3**, see scheme 3); Nickel is potentially redox-active, as copper(II), but it is diamagnetic under its (+II) oxidation state in a square planar environment. Consequently, both the one-electron oxidized and one-electron reduced forms are paramagnetic (S = ½) species. For such spin systems the nature of the magnetic orbitals (and the electronic structure of the compounds) could be unambigusouly established by EPR spectroscopy. By spectro-electrochemistry we show that **2** and **3** could be reversibly one-electron oxidized or reduced, affording stable monocations and monoanions, respectively. We unequivocally establish that both redox processes are ligand-centered, producing iminosemiquinonate-based and α-diimine radicals, respectively. In addition, we show that the anion radicals $\mathbf{2}^-$ and $\mathbf{3}^-$ readily react with dioxygen to produce the cations $\mathbf{2}^+$ and $\mathbf{3}^+$, respectively. **1** represents a particular case of tautomerization induced by metal coordination, which prevents the generation of persistent radical species. Finally, we investigated the catalytic activity of $\mathbf{2}^+$ towards aerobic oxidation of benzyl alcohol.

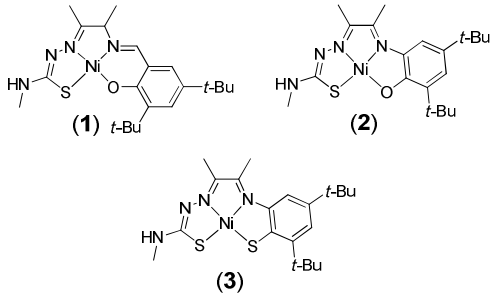

Scheme 3. Formula of the neutral complexes prepared.

Results

Synthesis and structural characterization of the neutral complexes.

1 was obtained in a one-pot synthesis by mixing the 2-(aminomethyl)-4,6-di-*tert*-butylphenol hydrochloride salt with diacetyl-mono-4-methyl-3-thiosemicarbazone[14e] and one equivalent of nickel(II) acetate (scheme 4). After few minutes a red precipitate formed, which was collected by filtration. As shown in Scheme 4a, **1** can exist under two tautomeric forms that correspond to either the α-diimine Mannich base or the Schiff base.

Complex **1** was crystallized by slow evaporation of a solution of the complex in MeOH/EtOH/CH_2Cl_2. The crystal cell of **1** contains two distinct molecules (A and B) whose structures do not differ significantly. The ORTEP view of one of these molecules, arbitrary chosen, is depicted in Figure 1a. It displays an almost square planar nickel(II) ion coordinated by two nitrogen atoms N1 and N2 (the former belongs to the salicylidene fragment), one sulfur S1 and the phenolato oxygen O1. The coordination bond distances Ni-N1, Ni-N2, Ni-S1 and Ni-O1 in molecule A are 2.175(1), 1.853(3), 1.852(3) and 1.835(2) Å, respectively (2.160(2), 1.847(3), 1.844(3) and 1.833(2) Å in molecule B). The Ni-S1 bond length is indicative of a thiolate rather than thiocarbonyl character of the sulfur atom. This is not unexpected since the thiocarbonyl groups of the semicarbazone units are known to easily tautomerize upon metal coordination. The Ni-O1 bond at 1.833-1.835 Å as well as the C1-O1 bond distance at 1.322(4) Å confirms the phenolato character of the aromatic ring.[9-11] Detailed analysis of the N-N and C-N bond distances reveals several important features. Firstly, the C9-N2 and C8-N1 bond lengths are unequivalent. The C7-N1 bond distance is 1.287(4) and 1.302(4) Å (in molecule A and B, respectively), while the N1-C8 is much longer, at 1.483(4) and 1.491(4) Å in molecule A and B, respectively. Secondly, one methyl group (attached to C9) is located 0.130 Å above the mean plane defined by the N1-N2-C8-C9-Ni atoms, while the other one

(attached to C8) resides 1.259 Å above this plane. Clearly, the C7-N1 bond is a double bond, while the N1-C8 one is a single bond. While tautomerization of the thiocarbonyl is common in semicarbazone complexes, tautomerization of the Mannich base into a salicylidene moiety is less described. It is likely the consequence of a higher acidity of the benzylic protons when compared to the methylenic protons of the bridge. Thus, **1** represents an interesting example of metal-promoted double tautomerization of the ligand, which is finally isolated under its thiolate / salicylidene form. It was important to check that tautomerization is not due to crystal packing. **1** was therefore dissolved in $CDCl_3$ and characterized by ^1H NMR. Its ^1H NMR spectrum displays clear resonances, showing that a single tautomer is present in solution. The fact that a resonance typical for an iminic proton is observed at 7.77 ppm, confirms the exclusive formation of the Schiff base tautomer in solution.

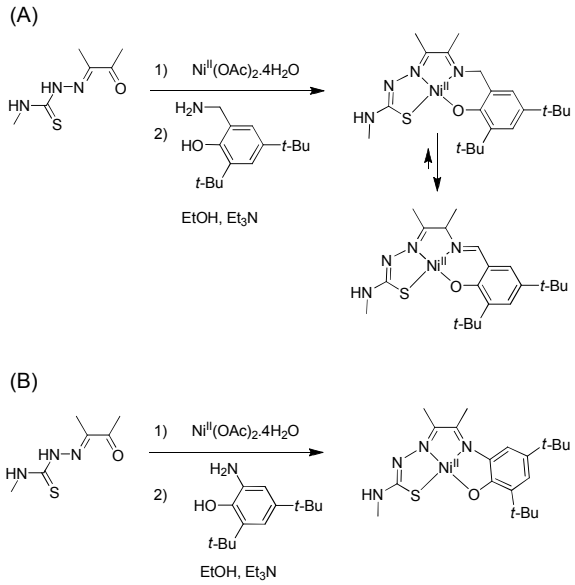

Scheme 4. Synthetic procedures.

Complexes **2** and **3** were obtained as single crystals by slow evaporation of a solution of the corresponding complex in MeOH/EtOH/CH_2Cl_2. The crystal structure of **2** is depicted in Figure 1b. The coordination bond distances Ni-O1, Ni-N1, Ni-N2 and Ni-S1 are 1.846(2), 1.870(2), 1.838(2), 2.173(1) Å, with a very small (< 2°) angle between the opposite O1-Ni-N1 and S1-Ni-N2 planes. The coordination bond lengths on the semicarbazone side compare fairly with those reported for symmetrical Ni(II) bis(thiosemicarbazone) complexes. [21] In contrast with **1**, the bridge displays the typical bonding pattern for an α-diimine moiety, with C7-N1 and C8-N2 bond distances of 1.307(3) and 1.313(3) Å, respectively, and a C7-C8 bond length of 1.487(3) Å. The C1-O1 and C6-N1 bond distances are 1.338(3) and 1.426(3) Å, with a C1-C6 bond length of 1.424(3) Å. All these features are consistent with an aminophenolate character of the aromatic ring. Noteworthy, Wieghardt *et al.* reported that the homoleptic NiL_2 complex depicted in Scheme 5 is best described by the diradical resonance form B. [22] In the case of **2** the C1-O1 and C2-N1 bond lengths are too long to support such a formulation. One can conlude that the thiosemicarbazone unit of **2** better stabilizes the ligand under its closed-shell electronic configuration.

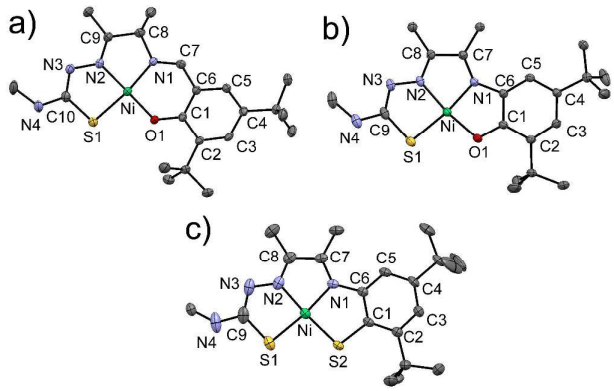

Figure 1. X-Ray crystal structures of: a) **1**; b) **2** ; c) **3** at the 30% ellipsoid probability. H atoms omitted for clarity.

Table 1. Coordination bond distances in **1**, **2** and **3** (in Å)

Complex	Method[a]	1	2	3
Ni-N1	XRD	1.843/1.852(3)	1.870(2)	1.880(3)
	DFT	1.843	1.864	1.882
Ni-N2	XRD	1.847/1.853(3)	1.838(2)	1.863(4)
	DFT	1.858	1.847	1.862
Ni-S1	XRD	2.160/2.175(1)	2.173(1)	2.160(1)
	DFT	2.194	2.184	2.183
Ni-O1	XRD	1.833/1.835(2)	1.846(2)	-
	DFT	1.853	1.877	-
Ni-S2	XRD	-	-	2.116(1)
	DFT	-	-	2.147

[a]: XRD: X-Ray diffraction data ; DFT: Calculations by using the BP86 functional.

The overall structure of **3** is similar to that of **2** (Figure 1c). The coordination bond distances Ni-S1, Ni-N1, Ni-N2 and Ni-S2 are 2.116(1), 1.880(3), 1.863(4) and 2.160(1) Å. Both the Ni-N1 and Ni-N2 bonds are slightly longer in **3** when compared to **2**. Regarding the aromatic ring, the C1-S2 and C6-N1 bond lengths are 1.773(4) and 1.425(6) Å, while the C-C ones fall within the range 1.38-1.41 Å. The absence of quinoid distribution of bond distances within the ring, combined with C7-N1 and C8-N2 bond distances at 1.320(5) and 1.295(7) Å within the bridge confirms that the ligand adopts a closed shell electronic configuration, similarly to **2**. Thus, **3** comprises both an aminothiophenolate and thiosemicarbazone moieties connected by an α,α-diimine bridge. Geometry optimizations were carried out on **1**, **2** and **3** by using the BP86 functional. As shown in Table 1 there is a good agreement between theoretical and experimental data. It is also gratifying that the evolution in coordination bond lengths within the series is fairly well predicted by calculations.

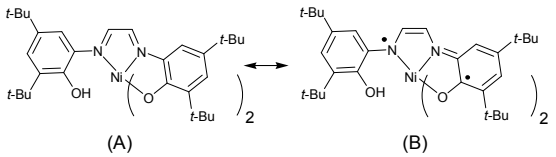

Scheme 5. Possible electronic structures for $Ni(L)_2$ (from reference 22).

Electrochemistry

The electrochemical behaviour of complexes **1**, **2** and **3** has been

studied by cyclic voltammetry (CV) in CH_2Cl_2 solution containing tetra-*n*-butyl ammonium perchlorate (TBAP) as supporting electrolyte. The CV curves of **1**, **2** and **3** are depicted in Figure 2.

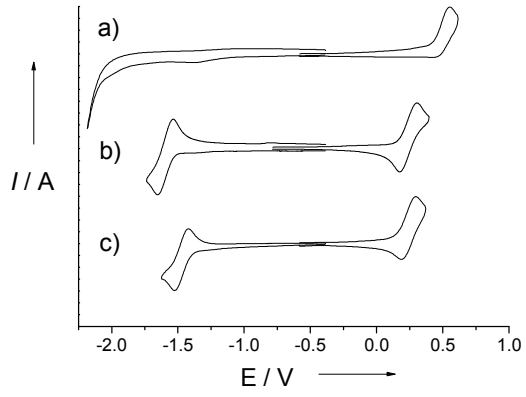

Figure 2. CV of 1 mM solutions of a) **1**, b) **2** and c) **3** in CH_2Cl_2 (+0.1 M TBAP). T = 298 K. The potentials are referenced versus the Fc^+/Fc redox couple.

Table 2. Electrochemical Properties of **1**, **2** and **3**[a]

Complex	Reduction		Oxidation		
	$E_{1/2}^c$	I_p^c/I_p^a [c]	$E_{1/2}^{a,1}$	$I_p^{a,1}/I_p^{c,1}$[c]	$E_p^{a,2}$
1			0.49 (irrev.)[b]		
2	-1.55(0.12)	2.35	0.26(0.23)	1.66	0.59 (irrev) [b]
3	-1.46(0.10)	3.16	0.22(0.11)	2.30	

[a] in volt vs. Fc^+/Fc

[b] irreversible process: $E_p^{a,1}$ is given.

[c] Determined at a scan rate of 0.1 V s^{-1}.

1 displays an irreversible oxidation wave at $E_p^{a,1}$ = 0.49 V without clear reduction wave down to -2 V. Based on literature data the anodic peak at $E_p^{a,1}$ is assigned to the oxidation of the phenolate moiety.[5-11,23] The phenoxyl/phenolate redox couple is unexpectedly irreversible, in contrast with what is commonly observed in Ni(II) salen complexes involving sterically hindered phenols. [23] This behaviour most likely results from to the higher lability of the proton of the Cβ (C7 in Fig. 1) in the salicylidene moieties, which favours decomposition of the radical cation $\mathbf{1}^+$.

The CV curve of **2** shows two oxidation waves, one being reversible at $E_{1/2}^{a,1}$ = 0.26 V vs Fc^+/Fc (Fig. 2) and the other being irreversible at $E_p^{a,2}$ = 0.59 V (not shown). Coulometric titration establishes that each wave corresponds to a one-electron process:

$$\mathbf{2}^{\bullet-} \overset{E_{1/2}^c}{\rightleftharpoons} \mathbf{2} \overset{E_{1/2}^{a,1}}{\rightleftharpoons} \mathbf{2}^{\bullet+} \xrightarrow{E_p^{a,2}} \text{Decomposition}$$

As it will be shown below the former corresponds to the oxidation of the *o*-aminophenolate moiety into an *o*-iminosemiquinonate radical. Owing to the irreversible nature of the second wave it was not possible to unambiguously assign the redox process. When scanning towards the cathodic region of potentials a reversible wave is observed at $E_{1/2}^c$ = -1.55 V. It is ascribed to the reduction of the α,α-diimine bridge into an α,α-diimine radical anion (see below).

The CV curve of **3** is closely related to that of **2**. It displays two reversible redox waves, one in oxidation at $E_{1/2}^{a,1}$ = 0.22 V and one in reduction at $E_{1/2}^c$ = -1.46 V. The latter is assigned to the α,α-diimine/α,α-diimine radical anion redox couple, similarly to **2**, while the former is ascribed to the oxidation of the *o*-aminothiophenolate into an *o*-iminothiosemiquinonate radical.

The oxidation potential $E_{1/2}^{a,1}$ at 0.22 V for **3** is similar to that measured for **2** (0.26 V). The fact that **2** and **3** are isostructural immediately leads to the conclusion that the nature of the heteroatom (X = S or O) has only a marginal effect on the oxidation potential. This conclusion could appear seemingly contradictory with a previous report by Wieghardt *et al.* who observed in a series of palladium complexes an easier oxidation of aminophenolato with respect to aminothiophenolato ligands. [24] Nevertheless, the different substitution pattern on the amino group complicated the comparison in this case, which may explain this trend. [24] In fact, the only noticeable difference in oxidation behaviour between **2** and **3** is the reversibility of the redox wave. Expressed as $I_p^{a,1}/I_p^{c,1}$ it is found to be smaller for **3**, attesting that the chemical stability of the thiosemiquinonate ligand is smaller. This behaviour follows the trend reported for phenylthiyl radicals, which have been reported to be less stable than their isoelectronic phenoxyl radical analogs. [25] Regarding the reduction wave, $E_{1/2}^c$ is observed at a potential substantially smaller for **2** than for **3**. The easier reduction of **3** results from the softer environment provided by the N_2S_2 coordination sphere.

Electronic spectra of the complexes

The electronic spectra of **2** and **3** are dominated by an absorption band at ca. 400-410 nm (figure 3, Table 3), which is assigned to a mixed ligand-to-ligand and metal-to-ligand charge transfer transition (see ESI).

The oxidized species $\mathbf{2}^+$ was generated by exhaustive electrolysis in CH_2Cl_2 (+ 0.1 M TBAP as supporting electrolyte) at 243 K. Upon oxidation the main band of **2** (406 nm [20040 $M^{-1}cm^{-1}$]) is red-shifted (417 nm [23 140 $M^{-1}cm^{-1}$]), while a shoulder appears at 466 nm (16910 $M^{-1}cm^{-1}$), as well as two broad bands at low energy: 635 nm (1720 $M^{-1}cm^{-1}$) and 773 nm (4360 $M^{-1}.cm^{-1}$). Based on their high intensity the bands above 600 nm are assigned to charge transfer transitions involving a ligand radical. Further support for this hypothesis comes from the close similarity between the Vis-NIR bands of $\mathbf{2}^+$ and the spectra of nickel(II) complexes involving iminosemiquinonate radicals. [26] Attempts to generate the cation $\mathbf{3}^+$ under similar conditions were unsuccessful, leading mainly to decomposition products. This result is in line with the lower reversibility of the oxidation wave of **3** in comparison to **2**.

The reduced species $\mathbf{2}^-$ and $\mathbf{3}^-$ were prepared *in situ* by reacting the neutral complexes **2** and **3** with a NaHg amalgam in THF under an argon atmosphere. The anion $\mathbf{2}^-$ displays bands at 410 (8390 $M^{-1}cm^{-1}$), 736 (2660 $M^{-1}cm^{-1}$) and 817 nm (2810 $M^{-1}.cm^{-1}$). The UV-Vis spectrum of $\mathbf{3}^-$ exhibits similar features, with an intense band at 422 nm (5180 $M^{-1}cm^{-1}$) and a lower intensity one at 836 nm (1470 $M^{-1}cm^{-1}$). These NIR absorption bands are evidence for the formation of a π-ligand radical species in both cases. [27] The exact nature of the orbitals involved in the transitions has been investigated by TD-DFT calculations for each species, as described below.

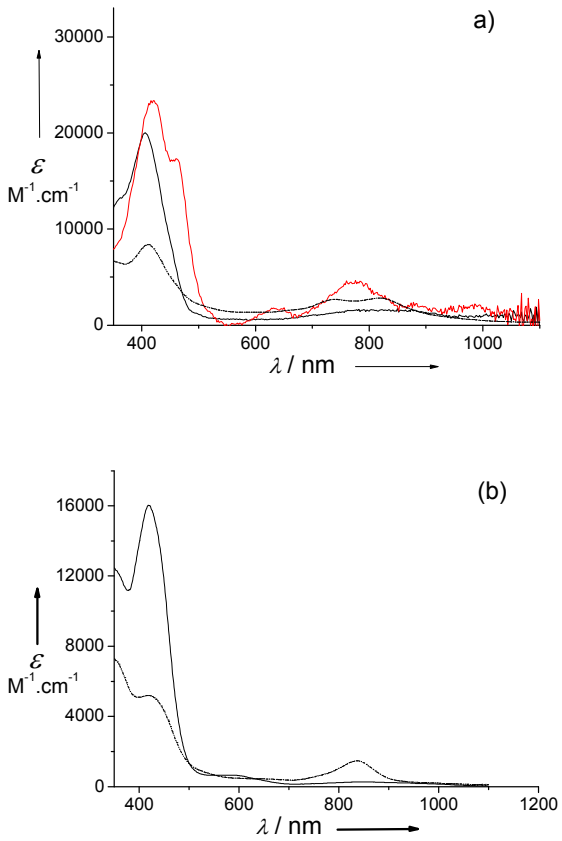

Figure 3. Vis-NIR spectra of solutions of the neutral and one-electron oxidized species in 0.05 mM CH_2Cl_2 solutions (+ 0.1 M TBAP in the case of 2^+): (a) **2** (black), 2^+ (red); (b) **3** (black); and of the one-electron reduced species in 0.05 mM THF solutions: (a) 2^- (doted black); (b) 3^- (dotted black). T = 298 K, except 2^+ (243 K).

Table 3. Electronic Spectral Data of the Complexes

Complex	λ [nm] (ε [M^{-1} cm^{-1}])
2	354sh (12630), 406 (20040), 825 br (1520) [a] *[379 (f = 0.35), 402 (f = 0.21), 820 (f = 0.06)]* [d]
2^+	417 (23140), 466 sh (16910), 635 (1720), 773 (4360) [b] *[388 (f = 0.57), 413 (f = 0.043), 530 (f = 0.026), 568 (f =* 0.046), 613 *(f = 0.041), 792 (f = 0.06), 1098 (f = 0.034)]* [d]
2^-	410 (8390), 736 br(2660), 817 br(2810) [c] *[394 (f =* 0.16), 410 *(f = 0.052), 905 (f = 0.037)]* [d]
3	421 (16020), 597 br (640) [a] *[390 (f = 0.049), 399 (f = 0.24), 412 (f = 0.076), 431 (f = 0.034), 606 (f = 0.006)]* [d]
3^-	422 (5180), 836 (1470) [c] *[413 (f = 0.048), 467 (f = 0.005), 572 (f = 0.006), 636 (f = 0.003), 912 (f = 0.014)]* [d]

[a] In CH_2Cl_2, at 298 K

[b] Electrochemically oxidized species in CH_2Cl_2 (+0.1 M TBAP) at 233 K

[c] Chemically reduced monoanionic species in THF at 298 K under Ar atmosphere.

[d] Italic: Calculated electronic excitations.

EPR Characterization

The EPR spectra of the chemically generated 2^- and 3^- have been recorded in frozen THF solution at 100 K. The EPR spectrum of 2^- consists of an almost isotropic signal centered at g_{iso} = 2.003 (figure 4). The fact that this g_{iso} is close to the free electron value argues against a Ni(I) formulation of the anion, which would give rise to much larger $g_{average}$ values (typically 2.11-2.25), with substantial g-anisotropy (Table 4). [28-30] Thus, 2^- consists of an anion radical coordinated to a diamagnetic Ni(II) metal ion. The spectrum is found to be relatively large, presumably due to unresolved hyperfine couplings. The EPR spectrum of 3^- is very similar to that of 2^-, although the isotropic g values is slightly higher (g_{iso} = 2.006). The difference in g_{iso} between 2^- and 3^- indicates that some delocalization of the unpaired electron occurs on the aminothiophenolate moiety, even though the radical has a main α-diimine character.

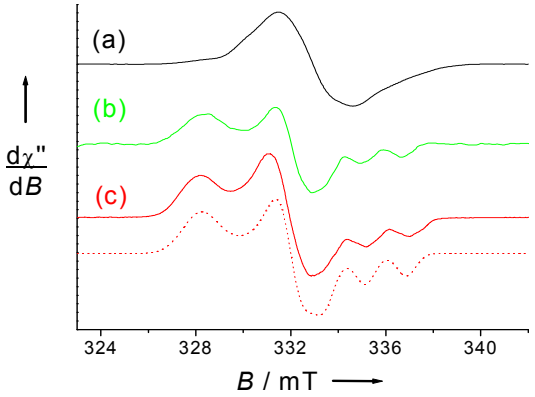

Figure 4. EPR spectra of 4 mM solutions of the chemically generated: a) 2^- (NaHg reduction in THF); b) 2^+ (silver oxidation in THF); c) 2^- after exposure to air. Solid lines: experimental spectra, dotted lines: simulation using parameters given in Table 2. Microwave freq. 9.33 GHz, power = 5 mW, mod. freq. 100 KHz, amp. 0.1 mT, T =100 K.

The EPR spectrum of 2^+ has been recorded both in CH_2Cl_2 (+ 0.1 M TBAP) solution (electrochemically generated cation) and THF (chemically generated using $AgSbF_6$) solutions. 3^+ could not be prepared under these conditions since it was found to be too unstable under electrolysis conditions and unreactive towards $AgSbF_6$ (likely because of the high affinity of the ligand for Ag^+).[13c] An efficient route to prepare both cations consists in generating the anions in THF in the glove box and exposing the solution to air.

Table 4. EPR parameters of the complexes 2^+, 2^-, $3^+$and 3^-

Complex	g_1, g_2, g_3 [A] (*calcd.*) [a]	g_{iso} (*calcd.*)
2^+(CH_2Cl_2)	2.059, 2.016, 1.996[52] *2.035, 2.015, 2.008*	2.024 (*2.019*)
2^+(THF)	2.034, 2.010, 1.992 [48] *2.035, 2.015, 2.008*	2.012(*2.019*)
2^-(THF)	*2.009, 2.001,1.989*[b]	2.003 *(2.000)*
3^+(THF)	2.069, 2.018, 1.986 [44] *2.069, 2.036, 2.016*	2.024 *(2.040)*
3^- (THF)	*2.015, 2.008, 1.989*[b]	2.006 (*2.004*)
[Ni^I(bphen)]	2.215, 2.070, 2.044 [c]	2.110
[$Ni^I(PPh_3)_3$](BF_4)	2.38, 2.12, 2.07 [d]	2.19
[Ni^I(NHC)(PPh_3)X]	2.275-2.405, 2.200-2.322, 2.034-2.073 [e]	2.254-2.182

[a] The hyperfine coupling constant A corresponds to a single ^{14}N nucleus (values given in MHz). DFT calculations were perfomed by using the B3LYP functional. The predicted values are indicated in italic.

[b] The g-anisotropy was unresolved, only g_{iso} is given.

[c] From reference 28.

[d] From reference 29.

[e] From reference 30.

The spectrum of the electrochemically generated species $\mathbf{2}^+$ in frozen CH_2Cl_2 (+0.1 M TBAP) displays a rhombic (S = 1/2) signal at $g_1 = 2.059$, $g_2 = 2.016$ and $g_3 = 1.996$ (Table 4). The g-anisotropy is much smaller than expected for a Ni(III) ion, [23,31] indicating that the cation is mostly a Ni(II)-semiquinonate radical species. The g_{iso} (2.023) is somewhat larger than 2.003-2.004, which are typical values for uncoordinated semiquinonate radicals. This indicates that the ligand π-orbital efficiently mixes with a t_{2g} orbital. As a consequence there is an admixture of orbital angular momentum in the ground state, resulting in deviation of the g_{iso} from the free electron value.

The EPR spectrum of $\mathbf{2}^+$ was also recorded in THF solution on two chemically oxidized samples (Table 4): One sample was generated by $AgSbF_6$ oxidation of **2**, while the other one was prepared by aerobic oxidation of $\mathbf{2}^-$. Both methods gave similar spectra, although the yield was smaller in the former case. This may be explained by the chelation of the Ag^+ cation by the thiosemicarbazone moiety. The spectrum consists of a well resolved rhombic (S = ½) signal, attesting that a single species is present in solution. The spectrum was satisfactorily simulated by using the following spin Hamiltonian parameters: $g_1 = 2.034$, $g_2 = 2.010$ and $g_3 = 1.992$. The g_{iso} value is again consistent with a main Ni(II)-semiquinonate radical character of the cation. It is worth noting that the high field component is split into a three-line pattern, as a result of hyperfine interaction with a single ^{14}N nuclear spin (I_N = 1). From simulation the hyperfine coupling constant $A_3 = 48$ MHz was obtained. The spectrum of $\mathbf{3}^+$ in THF differs only slightly from that of $\mathbf{2}^+$, confirming the main radical character of the complex. Thus, the change in donor set of the ligand does not affect the oxidation locus. The spectrum was simulated by adjusting the spin Hamiltonian parameters of $\mathbf{2}^+$, giving the set of values: $g_1 = 2.069$, $g_2 = 2.018$, $g_3 = 1.986$, with $A_3 = 44$ MHz for a single ^{14}N nucleus. The larger g-anisotropy and g_{iso} values determined for $\mathbf{3}^+$ in comparison to $\mathbf{2}^+$ deserves a comment. A deviation of the g values from the spin-only value (2.0023) and its orientation (g-anisotropy) is typically caused by the spin-orbit coupling and d-orbital admixture. The difference in g-values between $\mathbf{2}^+$ and $\mathbf{3}^+$ could be qualitatively explained by the larger spin-orbit coupling [32] and Z_{eff} [33] for the sulfur atom in comparison to the oxygen (ξ = 382 cm^{-1} vs. 151 cm^{-1}), and the fact that d-orbitals are energetically accessible in the former atom.

Theoretical investigations

In order to provide a clear picture of the electronic and geometric structures of **1**, **2** and **3** under their oxidized and reduced forms a computational investigation was carried out using density functional theory (DFT).

Before discussing the electronic structure of the cations and anions, we will focus on the molecular orbital (MO) diagram of the neutral compounds. The frontier MO diagram of **2** from a spin restricted B3LYP calculation is depicted in Figure 4. The HOMO of **2**, which basically corresponds to the SOMO of $\mathbf{2}^+$, is mainly ligand-centered (>80 %) and principally developed on the aromatic moiety. On the other hand, the LUMO of **2** (which corresponds to the SOMO of $\mathbf{2}^-$) is mainly centred on the α-diimine bridge. From this analysis it is clear that both oxidation and reduction of **2** involve ligand-centered orbitals. The cation $\mathbf{2}^+$ and the anion $\mathbf{2}^-$ are therefore expected to be radical species.

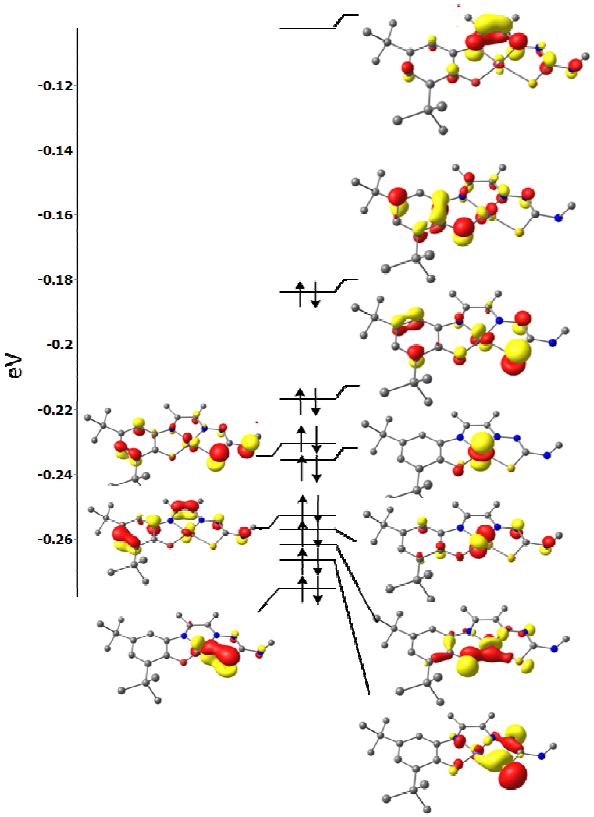

Figure 4. Frontier molecular orbital diagram of **2**

Let us now comment on the shape of the SOMO of $\mathbf{2}^+$ and $\mathbf{3}^+$ (figure 5). In both cases it is principally developed on the aromatic moiety, which makes these compounds iminosemiquinonate and iminothiosemiquinonate radical complexes, respectively. It is significant that the t_{2g} orbital contributes to the SOMO of $\mathbf{2}^+$ and $\mathbf{3}^+$ at ratio of 18 % and 20 %, respectively. This situation results from an efficient mixing (for symmetry reasons) between one out-of-plane $d_{xz/yz}$-orbital and the ligand π-orbital. Examination of the Mulliken spin populations in $\mathbf{2}^+$ and $\mathbf{3}^+$ (Table 5) reveals noticeable contributions of the C1, C4, C6 and X (O1 or S2) atoms (for the numbering see figure 1). Thus, the three canonical forms depicted in Scheme 6 contribute to the electronic structure of the cations.

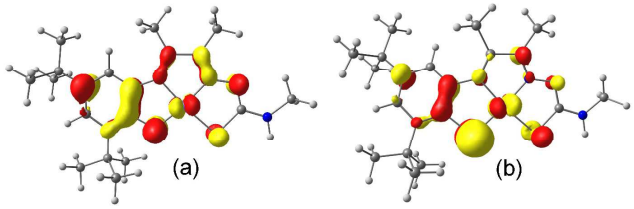

Figure 5. SOMOs of: a) $\mathbf{2}^+$ and b) $\mathbf{3}^+$ (doublet state) from a spin unrestricted BP86 calculation. The contribution to the SOMO are: (a) Ni : 18%; ligand : 82%. (b) Ni : 20%; ligand : 80%.

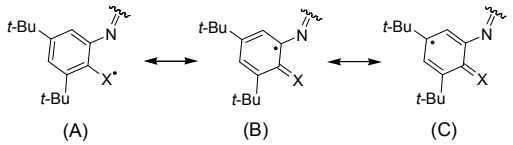

Scheme 6. Canonical forms of the cations $\mathbf{2}^+$ and $\mathbf{3}^+$

Further comparison between $\mathbf{2}^+$ and $\mathbf{3}^+$ reveals substantial differences in the individual contributions of the atoms. The spin populations on the C1, C2, C4 and C6 atoms are for instance smaller in $\mathbf{3}^+$ than in $\mathbf{2}^+$, whereas it is much higher on S2 than O1 (0.43 vs. 0.23). The weight of canonical form (A) is therefore larger for $\mathbf{3}^+$ than for $\mathbf{2}^+$. This situation resembles that encountered when anilinyl radicals are compared to the isoelectronic phenoxyl ones. For these free radicals it can be understood in terms of difference in electronegativity of the heteroatom X [34]: for X = O the singly occupied atomic orbital of the oxygen is lower-lying and interacts strongly with the benzene π-orbital; as a result the contribution of the oxygen atom to the SOMO decreases, at the expense of the benzene contribution. When X is less electronegative the singly occupied atomic orbital of the exocyclic group X interacts both with the π and π* orbitals of the benzene moiety. The contribution of the X group to the SOMO is consequently higher and the benzene contribution decreases concomitantly.

Table 5. Mulliken spin populations for a spin unrestricted B3LYP calculation [a]

Complex	$\mathbf{2}^+$	$\mathbf{2}^-$	$\mathbf{3}^+$	$\mathbf{3}^-$
Ni	0.08	0.04	0.15	0.05
O1 or S2	0.23	0.00	0.43	-0.01
C1	0.08	0.07	0.05	0.07
C2	0.06	-0.03	0.03	-0.03
C3	-0.01	0.09	0.00	0.07
C4	0.20	-0.04	0.12	-0.03
C5	-0.09	0.08	-0.05	0.06
C6	0.16	-0.05	0.10	-0.03
N1	0.00	0.18	0.03	0.14
C7	0.04	0.21	0.00	0.27
C8	0.01	0.06	0.05	0.01
N2	0.05	0.27	0.00	0.29
N3	0.10	-0.03	0.04	-0.02
C9	0.00	0.11	0.00	0.10
S1	0.05	0.00	0.06	0.00
N4	0.03	0.04	0.00	0.05

[a] For atom numbering see Figure 1

The calculated SOMO for $\mathbf{2}^-$ and $\mathbf{3}^-$ are depicted in Figure 6. As for the cations the SOMO is mainly ligand-centered (>89 %). The metal contribution is somewhat smaller in the anions as it does not exceed 11%. It again arises from the mixing between the radical π-orbital and the second out-of-plane t_{2g} orbital. The SOMO is largely developed on the α-diimine bridge, with some extend on the N1,C3 and C5 atoms of the aromatic ring and the thiosemicarbazone unit. It is interesting that the SOMO is unsymmetrically distributed over the α-diimine bridge in $\mathbf{3}^-$ as it is "pulled" by the aminothiophenolate group. One may therefore expect differences in the stabilization of the anions by resonance, and ultimately in the redox potentials, as experimentally observed. Examination of the Mulliken spin populations confirms the α-diimine radical character of both anions, with populations at 0.18, 0.27 ($\mathbf{2}^-$) and 0.14, 0.29 ($\mathbf{3}^-$) for the N1 and N2 atoms, respectively. Analysis of the bonding pattern within the α-diimine bridge provides insight onto the geometrical rearrangement resulting from reduction: The SOMO of the anions (which formally corresponds to the LUMO of the neutral species) features a C-N bond that is anti-bonding in nature and a C-C bond that is bonding (Scheme 7). In the HOMO of the neutral compounds, the C-C bond is anti-bonding and the C-N bond is bonding. Since the LUMO becomes populated upon reduction of **2** into $\mathbf{2}^-$ an increase in the C-N bond length and a decrease in the C-C bond distance would be expected. This simple description is corroborated by the geometry optimized structures: the C-N bond is predicted to be 0.03 Å larger in the anion (from 1.33 to 1.36 Å), while the C-C bond is shortened by 0.04 Å in the anion (from 1.46 to 1.42 Å).

In order to validate our approach, EPR calculations on the optimized structures of $\mathbf{2}^+$, $\mathbf{2}^-$, $\mathbf{3}^+$ and $\mathbf{3}^-$ have been performed. The calculated g-tensors are given in Table 4. The lowest g value (g_3) is assigned to g_z, with the z-axis pointing orthogonally to the plane of the molecule, while the highest (g_1) is g_x and points roughly along the Ni-X axis (X = O1 or S2). Consistent with experimental findings, the computed $\Delta g = g_1 - g_3$ is found to be larger for the cations (0.025 and 0.050 for $\mathbf{2}^+$ and $\mathbf{3}^+$, respectively) than for the anions (0.019 and 0.025 for $\mathbf{2}^-$ and $\mathbf{3}^-$, respectively). In addition, the g_{iso} value is larger for the cations than for the anions. This result is in line with the smaller metal contribution to the SOMO in the anions in comparison to the cations (see above). If we now focus on the cations, the larger g_{iso} and g-anisotropy observed for $\mathbf{3}^+$ in comparison to $\mathbf{2}^+$ are in agreement with the larger spin-orbit coupling of the sulfur atom when compared to oxygen.[32]

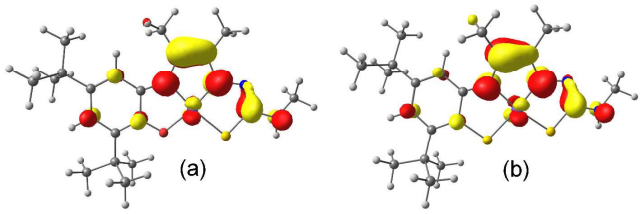

Figure 6. SOMOs of: a) $\mathbf{2}^-$ and b) $\mathbf{3}^-$ (doublet state) from a spin unrestricted BP86 calculation. The contribution to the SOMO are: (a) Ni : 10%; ligand : 90%. (b) Ni : 11%; ligand : 89%.

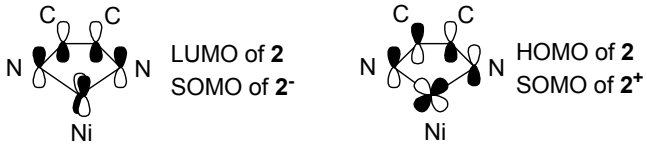

Scheme 7. Picture of the frontier orbitals in the α-diimine bridge of $\mathbf{2}^+$, **2** and $\mathbf{2}^-$.

TD-DFT investigation

The exact nature of the orbitals involved in the UV-vis transitions of **2**, **3**, $\mathbf{2}^+$, $\mathbf{2}^-$ and $\mathbf{3}^-$ was investigated by TD-DFT calculations. Difference transition density plots for the computed transitions are shown in the electronic supplementary information.

For **2** the principal electronic excitations that contribute to the main absorption at 406 nm and the weak band at 825 nm are

computed at λ_{calc} = 379 nm (f = 0.35), λ_{calc} = 402 nm (f = 0.21) and λ_{calc} = 820 nm (f = 0.06), see Table 3. The acceptor fragment is, as expected, mainly the α-diimine fragment in all three cases. The donor orbital has a significant aminophenolate character in the excitation predicted at 820 nm, which mainly corresponds to the HOMO→LUMO transition. The intense band at 379 nm contains a significant amount of d_{xz} to α-diimine MLCT character, while the 402 nm one is mostly a LLCT.

For **3** the only significant electronic excitation in the low energy domain is predicted at 606 nm, but the oscillator strength is very small (f = 0.006). Thus, the principal electronic excitations that contribute to the Vis-NIR spectrum of **3** are ligand-to-α-diimine CT bands at λ_{calc} = 412 and 399 nm, as well as a metal-to-α-diimine CT band at 390 nm.

For $\mathbf{2}^+$ the principal electronic excitation is predicted at 388 nm (LLCT transition, f = 0.57). A lower intensity band is predicted at 413 nm (dd transition, f = 0.043). They reproduce the experimental red shift of the main bands of **2** during oxidation. In addition, several new bands (mostly LLCT) of moderate intensity are predicted at 530 nm (f = 0.026), 568 nm (f = 0.046), 613 nm (f = 0.041), 792 nm (f = 0.060) and 1098 nm (f = 0.034), in agreement with experimental data. The lowest energy transition deserves a comment. The donor orbital (HOMO) is mainly localized on the sulfur atom of the semicarbazone unit while the acceptor one (SOMO) is principally developed on the iminosemiquinonate ring (although some delocalization exists, see figure 5). Thus, the excited state corresponds to a thiyl radical localized on the semicarbazone unit, according to Scheme 8.

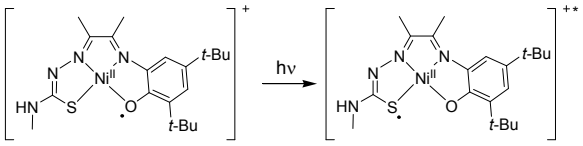

Scheme 8. Lowest energy electronic excitation of $\mathbf{2}^+$

In $\mathbf{2}^-$, the principal electronic excitations that contribute to the experimental bands at 410 (8390 $M^{-1}.cm^{-1}$) and 817 nm (2810 $M^{-1}.cm^{-1}$) are LLCT transitions, which are calculated at λ_{calc} = 394 nm (f = 0.16), λ_{calc} = 410 nm (f = 0.052) and λ_{calc} = 905 nm (f = 0.037) (Table 3). They involve predominantly delocalized π orbitals with some extend on the metal center (non-negligible d character). Noteworthy, calculations predict correctly the lower intensity of the band at *ca*. 400 nm on going from **2** to $\mathbf{2}^-$.

Regarding $\mathbf{3}^-$, calculations reproduce the decrease in intensity of the band at *ca*. 420 nm upon reduction of **3** (λ_{calc} = 413 nm, f = 0.048). They also predict the appearance of a transition of low intensity in the NIR region (λ_{calc} = 912 nm, f = 0.014), whose nature is similar to that computed at 905 nm for $\mathbf{2}^-$. The good agreement between experiment and theory further supports the description of the cations and anions as radical species.

Benzyl alcohol oxidation

Owing to the ability of **2** to shuttle between a phenoxyl-based radical state and a two-electron reduced state, as GO, we investigated its reactivity towards aerobic oxidation of benzyl alcohol. The conditions were 1 mM of catalyst (equimolar mixture of **2** and $AgSbF_6$), 20 mM of *tert*-BuOK and benzyl alcohol in dry CH_2Cl_2. After 20 hours stirring at 298 K under a constant dioxygen pressure of 2 bars the reaction mixture was analyzed by GC. For an initial substrate concentration of 0.1 M we observed the conversion of 13% of benzyl alcohol into benzaldehyde. It is clear that air acts as a co-oxidant since the yield in benzaldehyde is much higher than the amount of $AgSbF_6$ initially added. Inspection of the reaction mixture after 20 hours reveals a total bleaching of the solution, whose initial color cannot be restored by addition of base. Bleaching is therefore not associated with protonation of the complex, as observed in some salen-type compounds, [5b,5c,6b,6c,7c,7d] but rather with decomposition of the catalyst. This hypothesis is further supported by the fact that catalysis is not improved in the presence of a higher amount of substrate (up to 25 % in volume). In order to compare $\mathbf{2}^+$ with published biomimetic models of GO we evaluated the catalytic efficiency of some copper(II) radical salen complexes (ligands: *N,N'*-bis{3-*tert*-butyl-5-methoxysalicylidene}phenylene-1,2-diamine and *N,N'*-bis{3-*tert*-butyl-5-methoxysalicylidene}cyclohexane-1,2-diamine) [5c,6b] under similar experimental conditions. The conversion was systematically lower for the copper(II) radical salen complexes (<5%). The higher catalytic efficiency of $\mathbf{2}^+$ may be explained by the tristability of **2**, which contributes to the protection of the catalyst against disproportionation and metal release. The reaction likely proceeds in a ping-pong mechanism similarly to GO: [3] $\mathbf{2}^+$ reacts with the deprotonated alcohol to give benzaldehyde and the two-electron reduced form of the catalyst $\mathbf{2}^-$. Species $\mathbf{2}^-$ is then oxidized by molecular dioxygen to regenerate the active catalyst (Scheme 9). All together these results show that **2** efficiently uses air as an oxidant to promote oxidation of benzyl alcohol into aldehyde as does GO.

Discussion and conclusion

In this article we describe the preparation of square planar nickel(II) complexes of three unsymmetrical thiosemicarbazone-based ligands featuring a sterically hindered salicylidene (**1**), aminophenol (**2**) or thiophenol (**3**) moiety. Species **1** was prepared by condensation of the 2-(aminomethyl)-4,6-di-*tert*-butylphenol hydrochloride salt with diacetyl-mono-4-methyl-3-thiosemicarbazone. Although in the early stage of the reaction a Mannich base is obtained, it easily tautomerizes into the most stable salicylidene form. This result is explained by the higher acidity of the benzylic protons in comparison to the aliphatic protons of the α-diimine bridge. Thus, **1** represents an uncommon example of metal-promoted double tautomerization of the ligand, where the thiocarbonyl is converted into a thiolate group and the Mannich base into a Schiff base. It is interesting to compare the redox behaviour of **1** with that of nickel salen complexes (involving similar di-*tert*-butyl phenolate moieties), which are known to support a ligand-centered oxidative chemistry. The phenoxyl/phenolate redox couple (0.49 V vs. Fc^+/Fc for **1**) is observed within the same potential window in both families of compounds, attesting that the nature of the redox-active fragment is similar (salicylidene in both cases). Surprisingly, the redox wave was found to be irreversible for **1**, whereas it is fully reversible in the salen family. This result is interpreted by the presence of an acidic hydrogen in the vicinity of the oxidized salicylidene moiety of **1**. Another instructive comparison could be made with the nickel complex described a couple of years ago by Arion *et al.* (compound E in Scheme 1). They reported a

substantially higher value for the phenoxyl/phenolate redox couple (0.67 V). The thermodynamic stability of the radical is therefore lower, although the redox system remains reversible. This behaviour is likely a consequence of the larger spin delocalization in their complex. All these electrochemical results show that **1** is unfortunately not robust enough towards oxidation to mimick the GO reactivity. Complex **1** was also the most difficult compound to reduce within this series, with a E_p^c that is lower than -2 V. This value is well below those reported for the reduction of copper(II) complexes of tetradentate bis(thiosemicarbazone) ligands (-0.97 V vs. Fc^+/Fc for the [Cu(ATSM)] complex). Clearly, **1** does not benefit from the stabilizing ability of the semicarbazone unit for low oxidation states of the complex. This underlines the crucial role of the α-diimine bridge in the stabilization of the low valent copper ion in these families of compounds.

Species **2** and **3** were structurally characterized, showing a square planar nickel ion. It is striking that **2** displays reversible monoelectronic redox waves both in oxidation and reduction ($E_{1/2}$ = 0.26 and -1.55 V vs Fc^+/Fc, respectively), although the N_2SO donor set is similar to **1**. By EPR and UV-Vis spectroscopies, as well as DFT calculations we established that both the oxidation and reduction products ($\mathbf{2}^+$ and $\mathbf{2}^-$, respectively) are radical species. The cation $\mathbf{2}^+$ has a main iminosemiquinonate character, with minor contribution of the α-dimine bridge. The anion $\mathbf{2}^-$ exhibits a dominant α-diimine π-radical character, with partial delocalization over the aromatic ring on one side and the conjugated imine of the thiosemicarbazone fragment on the other side. It is significant that $\mathbf{2}^-$ readily reacts with dioxygen to form the cation $\mathbf{2}^+$ (Scheme 9). This chemistry is in line with the GO's one, which reacts with O_2 under its reduced form to regenerate the phenoxyl radical state of the enzyme. As GO the cation $\mathbf{2}^+$ oxidizes benzyl alcohol to benzaldehyde by using dioxygen as co-oxidant. Although the yield is moderate (13 % for a substrate concentration of 0.1 M) it is significantly higher than that measured under similar conditions for copper(II) radical salen complexes.

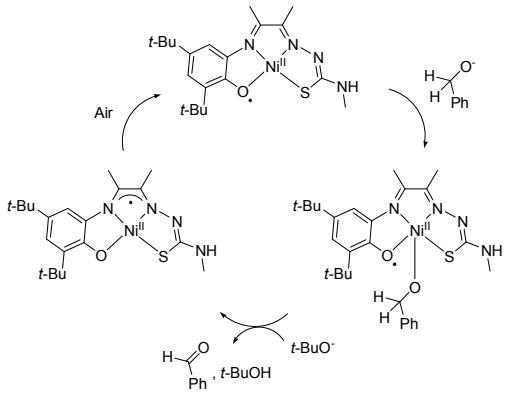

Scheme 9. Aerobic oxidation of benzylalcohol by complex $\mathbf{2}^+$

Compound **3** was found to be almost isostructural with **2**, the most noticeable differences between the two complexes being the Ni-X and C1-X bond distances (where X denotes O1 and S2 in **2** and **3**, respectively). Similarly to **2**, **3** could be reversibly one-electron oxidized (into $\mathbf{3}^+$) and one-electron-reduced (into $\mathbf{3}^-$). Species $\mathbf{3}^+$ is assigned to an iminothiosemiquinonate radical, while $\mathbf{3}^-$ displays the same electronic structure than $\mathbf{2}^-$ and comprises a α-diimine π-radical fragment. By comparing $\mathbf{2}^+$ with $\mathbf{3}^+$ one can notice several important features: firstly, the redox potentials $E_{1/2}^{a,1}$ are remarkably similar, although the Ni-X bond distance is 0.3 Å longer in $\mathbf{3}^+$ and the covalency is dramatically different. This important observation shows that the nature of the heteroatom (X = S or O) has only a marginal effect on the oxidation potential of the radical precursor. Secondly, the individual contribution of the atoms to the SOMO are substantially different. The most salient features are a larger calculated Mulliken spin population at X (O1 or S2) and Ni atoms and smaller spin population at the C1, C2 and C4 atoms (C_{ipso}, C_{ortho} and C_{para}, respectively) in $\mathbf{3}^+$ in comparison to $\mathbf{2}^+$. The difference in electronic structure between these two radicals and the peculiarity of the sulfur atom could be experimentally probed by EPR spectroscopy. The two radicals indeed exhibit a different g-anisotropy that could be qualitatively explained in terms of a larger spin-orbit coupling and Z_{eff} for the sulfur atom when compared to the oxygen, and the fact that d-orbitals are energetically accessible only in the sulfur case. Lastly, one could comment on the relative stability of the radical cations: while iminosemiquinonate radicals could be quantitatively prepared by bulk electrolysis at 243 K, the iminothiosemiquinonate radical did not. The iminothiosemiquinonate radicals are therefore chemically less stable than then iminosemiquinonate counterparts, although the themodynamic stabilization of both radicals (reflected by the $E_{1/2}^{a,1}$ potential) is identical.

In addition to its ligand-based oxidative chemistry, **3** supports a ligand-centered redox chemistry in reduction, affording the α-diimine radical species $\mathbf{3}^-$. The electronic structure of $\mathbf{3}^-$ being closely related to that of $\mathbf{2}^-$, **2** and **3** constitute valuable models to study the influence of the donor set (N_2S_2 vs. N_2SO) on the reduction potential $E_{1/2}^c$. The replacement of a single O^- donor by a S^- donor induces an anodic shift of the reduction wave by 0.08 V (-1.46 V for **3** vs. -1.58 V for **2**). This behaviour follows the trend in polarizability of the atoms: the sulfur being more polarisable (softer) than the oxygen it is more prone to stabilize low oxidation states of the complex.

In conclusion, the association of three units of different nature (thiosemicarbazone, α-diimine and aminophenol or aminothiophenol) in a single ligand confers to the corresponding nickel complexes a rich redox chemistry. With this ligand design both oxidation and reduction processes are accessible and reversible, albeit the SOMO has a different location (in the cation and anion, respectively). We establish that **2** catalyzes aerobic oxidation of benzyl alcohol, the ligand supporting the redox events. This opens new perspectives in the design of catalysts employing redox non-innocent ligands for various chemical transformations.

Experimental section

Materials and Instruments

Anhydrous tetrahydrofurane or dichloromethane (> 99.8 %) used for electrochemistry and spectroscopic characterization were purchased from Sigma-Aldrich and stored in the glovebox. X-Band EPR spectra were recorded on a BRUKER EMX Plus spectrometer controlled with the Xenon software and equipped with a Bruker teslameter. A Bruker nitrogen flow cryostat

connected to a high sensitivity resonant cavity was used for 100 K measurements. The spectra were simulated using the SIMFONIA software (BRUKER). NMR spectra were recorded on a Bruker AM 300 (^{1}H at 300 MHz, ^{13}C at 75 MHz) or a Bruker Avance 400 (^{1}H at 400 MHz, ^{13}C at 100 MHz). Chemical shifts are given relative to solvent residual peak. Mass spectra were recorded on a Bruker Esquire 3000 (ESI/Ion Trap) equipment. Microanalysis were performed by using an apparatus designed by the Service Central d'Analyse du CNRS (Lyon, France). 298 K UV/Vis/NIR spectra were recorded on a Perkin–Elmer Lambda 1050 spectrophotometer equipped with a temperature controller unit set at 298 K. The quartz cell path length is 1.000 cm. Cyclic voltammetry curves were recorded on a CHI 620 potentiostat in a standard three-electrode cell under Argon atmosphere. An $AgNO_3$/Ag (0.01 M) reference electrode was used. All the potentials given in the text are referred to the regular Fc^+/Fc redox couple used as external reference. A vitreous carbon disc electrode (5 mm diameter) polished with 1 mm diamond paste was used as working electrode. Electrolysis was performed on a PAR 273 potentiostat, under Argon atmosphere at 233 K, using a carbon felt working electrode. Catalytic experiments were performed under a dioxygen atmosphere (2 bars) during 20 hours in a HEL's High Pressure ChemSCAN reactor. The reaction mixture was then analyzed by gas chromatography (Shimadzu) after filtration. Benzaldehyde concentration was determined by using mesitylene as an internal standard.

Crystal structure analysis

A single crystal of **1**, **2** or **3** was coated with perfluoropolyether, picked up with nylon loops and mounted in the nitrogen cold stream of the diffractometer. Mo-Kα radiation (λ=0.71073Å) from a Mo-target rotating-anode X-ray source equipped with INCOATEC Helios mirror optics was used. Final cell constants were obtained from least squares fits of several thousand strong reflections. Intensity data were corrected for absorption using intensities of redundant reflections with the program SADABS.[35] The structures were readily solved by Patterson methods and subsequent difference Fourier techniques. The OLEX software [36] was used for the refinement. All non-hydrogen atoms were anisotropically refined and hydrogen atoms were placed at calculated positions and refined as riding atoms with isotropic displacement parameters.

Computational details

All electronic structure calculations presented were carried out using the ORCA program package.[37] Full geometry optimizations were performed for all complexes using the GGA functional BP86 [38-40] in combination with the Def2-TZV/P [41] basis set for all atoms and by taking advantage of the resolution of the identity (RI) approximation in the Split-RI-J variant [42] with the appropriate Coulomb fitting sets. [43] Increased integration grids (Grid4 in ORCA convention) and tight SCF convergence criteria were used. Solvent effects were accounted for according to the experimental conditions. For that purpose, we used the CH_2Cl_2 (ε = 38.3) or THF (ε = 7.25) solvent according to the experimental conditions within the framework of the conductor like screening (COSMO) dielectric continuum approach. [44] The relative energies and epr parameters were obtained from single-point calculations using the B3LYP functional [45,46] together with the Def2-TZV/P [41] basis set. They were computed from the gas-phase optimized structures as a sum of electronic energy, thermal corrections to free energy, and free energy of solvation. Optical properties were also obtained from single-point calculations using the hybrid functional B3LYP [45,46] and the Def2-TZV/P [41] basis set. Electronic transition energies and dipole moments for all models were calculated using time-dependent DFT (TD-DFT) [47] within the Tamm-Dancoff approximation. [48,49] To increase computational efficiency, the RI approximation [50] was used in calculating the Coulomb term and at least 30 excited states were calculated in the TDDFT calculations.

Preparation of the complexes

1. To a solution of diacetyl-mono-4-methyl-3-thiosemicarbazone [12b] (0.150 g, 0.87 mmol) dissolved in EtOH (15mL) was added $Ni(OAc)_2$•$2H_2O$ (0.211 g, 0.87 mmol) and Et_3N (481 µL, 3.48 mmol) in EtOH (5 mL). After few minutes of stirring, a solution of 2-(aminomethyl)-4,6-di-*tert*-butylphenol (0.236 g, 0.87 mmol) dissolved in 10 mL of EtOH was added to the resulting red solution. The solution was stirred at reflux for 1h. The resulting red precipitate was filtered, dissolved in acetone, stirred at room temperature for 10 min, filtered over a plug of celite and concentrated. Yield: 0.195 g, (50 %). Anal. Calc. for $C_{20}H_{30}N_4NiS$: C, 56.39; H, 7.21; N, 12.53; S, 7.17; O, 3.58. Found: C, 56.21; H, 7.18; N, 12.51; S, 7.30; O, 3.54. ESI-MS m/z: 447.1 $[M+H]^+$. ^{1}H NMR ($CDCl_3$, 300 MHz) (ppm): 7.77 (s, 1H), 7.29 (d, ^4J = 2.7 Hz, 1H), 6.95 (d, ^4J = 2.4 Hz, 1H), 4.50 (m, br, 1H), 3.11 (m, br, 1H) 2.92 (d, ^3J = 4.8 Hz, 3H), 2.17 (s, 3H), 1.55 (d, ^3J = 6.9 Hz, 3H), 1.26 (s, 9H), 1.24 (s, 9H).

2. To a solution of diacetyl-mono-4-methyl-3-thiosemicarbazone (0.195 g, 1.13 mmol) dissolved in EtOH (20mL) was added $Ni(OAc)_2$•$2H_2O$ (0.28 g, 1.13 mmol) and a few drops of Et_3N in EtOH (5mL). After few minutes of stirring, a solution of 2-amino-4,6-di-*tert*-butylphenol [51] (0.25 g, 1.13 mmol) dissolved in 10 mL of EtOH was added to the resulting brown solution. The solution was stirred at reflux for 1h. The resulting red precipitate was filtered and washed with cold EtOH. Yield: 0.333 g, (68 %). Anal. Calc. for $C_{20}H_{30}N_4NiOS$: C, 55.45; H, 6.98; N, 12.93; S, 7.40; O, 3.69. Found: C, 55.63; H, 7.01; N, 12.99; S, 7.01; O, 3.54. ESI-MS m/z: 433.1 $[M+H]^+$. ^{1}H NMR (DMSO d_6, 300 MHz) (ppm): 7.98 (q, br, 1H), 6.80 (s, 2H), 2.75 (d, ^3J = 4.5 Hz, 3H), 2.20 (s, 3H), 1.80 (s, 3H) 1.17 (s, 9H), 1.09 (s, 9H).

3. To a solution of diacetyl-mono-4-methyl-3-thiosemicarbazone (0.1 g, 0.58 mmol) dissolved in EtOH (15mL) was added $Ni(OAc)_2$•$2H_2O$ (0.1 g, 0.58 mmol) and Et_3N (321 µL, 2.32 mmol) in EtOH (5mL) under an inert atmosphere. After few minutes of stirring, a solution of 2-mercapto-3,5-di-*tert*-butylaniline [52] (0.144 g, 0.58 mmol) dissolved in few mL of EtOH was added to the resulting brown solution. The solution was stirred at reflux for 1h and stirred at room temperature overnight under an inert atmosphere. The resulting dark brown precipitate was filtered, dissolved in acetone, stirred at room temperature for 10 min, filtered over a plug of celite and concentrated. Yield: 0.116 g, (62%). Anal. Calc. for $C_{20}H_{30}N_4NiS_2$: C, 53.46; H, 6.73; N, 12.47; S, 14.27. Found: C, 52.98; H, 6.71; N, 12.63; S, 14.32. ESI-MS m/z: 449.1 $[M+H]^+$. ^{1}H NMR (DMSO d_6, 300 MHz) (ppm): 8.23 (q, br, ^3J = 4.2 Hz,

1H), 7.02 (s, br, 1H), 6.81 (s, br, 1H), 2.89 (d, ^3J = 4.2 Hz, 3H), 2.32 (s, 3H), 1.95 (s, 3H), 1.43 (s, 9H), 1.23 (s, 9H).

Acknowledgments

We thank the Labex Arcane (ANR-11-LABX-0003-01, Université Joseph Fourier, Grenoble) for financial support.

Notes and references

[a] *Département de Chimie Moléculaire - Chimie Inorganique Redox Biomimétique (CIRE) - UMR CNRS 5250, Université J. Fourier, B. P. 53, 38041 Grenoble cedex 9 (France); E-mail: fabrice.thomas@ujf-grenoble.fr*

[b] *Max Planck Institute for Chemical Energy Conversion, Stiftstrasse 34-36, D-45470 Mülheim an der Ruhr, Germany.*

† Electronic Supplementary Information (ESI) available: X-ray crystallographic files of complexes **1**, **2**, **3** (CCDC 1043950-1043952), DFT optimized structures, spin density plots, TD-DFT assignment of the UV-Vis bands and EPR spectra. See DOI: 10.1039/b000000x/

1 See the recent Special Issues of *Inorg. Chem.* on Redox-Active ligands (2011, **Vol. 50**, Issue 20, Pages: 9737-9903) and *Eur. J. Inorg. Chem.* on Cooperative & Redox Non-Innocent Ligands in Directing Organometallic Reactivity (2012, Issue 3, Pages 340-580). See also excellent review articles: a) R. G. Hicks, *Org. Biomol. Chem.* 2007, **5**, 1321. b) W. Kaim, B. Schwederski, *Coord. Chem. Rev.* 2010, **254**, 1580. c) W. I. Dzik, J. I. van der Vlugt, J. N. H. Reek, B. de Bruin, *Angew. Chem. Int. Ed.* 2011, **50**, 3356. d) R. A. Luca, R. H. Crabtree, *Chem. Soc. Rev.* 2013, **42**, 1440.

2 a) H. J. Krüger, *Angew. Chem. Int. Ed.* 1999, **38**, 627. b) B. A. Jazdzewski, W. B. Tolman, *Coord. Chem. Rev.* 2000, **200-202**, 633. c) S. Itoh, M. Taki, S. Fukuzumi, *Coord. Chem. Rev.* 2000, **198**, 3. J. L. Pierre, *Chem. Soc. Rev.* 2000, **29**, 251. d) P. Chaudhuri, K. Wieghardt, *Prog. Inorg. Chem.* 2001, **50**, 151. e) F. Thomas, *Eur. J. Inorg. Chem.* 2007, 2379. f) R. G. Hicks, *Angew. Chem. Int. Ed.* 2008, **47**, 7393. g) F. Thomas, in *Stable Radicals: Fundamentals and Applied Aspects of Odd-Electron Compounds,* R. G. Hicks, Ed.; John Wiley and Sons: Chichester, 2010, pp 281. h) P. J. Chirik, K. Wieghardt, *Science* 2010, **327**, 794. i) Y. Shimazaki, O. Yamauchi, O. *Ind. J. Chem.* 2011, 383. j) C. T. Lyons, T. D. P. Stack, *Coord. Chem. Rev.* 2013, **257**, 528. k) Y. Shimazaki, *Adv. Mat. Phys. Chem.* 2013, **3**, 60.

3 a) J. W. Whittaker, in *Metal Ions in Biological Systems*, ed Sigel, H. and Sigel, A., Marcel Dekker, New-York, 1994, vol. **30**, pp. 315. b) C. D. Borman, C. G. Saysell, A. Sokolowski, M. B. Twitchett, C. Wright, A. G. Sykes, *Coord. Chem. Rev.* 1999, **190-192**, 771. c) M. J. McPherson, M. R. Parsons, R. K. Spooner, C. M. Wilmot, in *Handbook for metalloproteins*, ed A. Messerschmidt, R. Huber, T. Poulos, K. Wieghardt, John Wiley and Sons, 2001, **vol. 2**, pp. 1272. d) J. W. Whittaker, in *Advances in Protein Chemistry*, ed F. M. Richards, D. S. Eisenberg, J. Kuriyan, Academic Press, Elsevier, 2002, **vol. 60**, pp. 1. e) J. W. Whittaker, *Chem. Rev.* 2003, **103**, 2347. f) M. S. Rogers, D. M. Dooley, *Curr. Opin. Chem. Biol.* 2003, **7**, 189. g) S. J. Firbank, M. Rogers, R. Hurtado-Guerrero, D. M. Dooley, M. A. Halcrow, S. E. V Phillips, P. F. Knowles, M. J. McPherson, *Biochem. Soc. Trans.* 2003, **31**, 506.

4 a) J. N. Lopez-Rodriguez, J. Hernandez-Ruiz, F. Garcia-Canovas, R. N. F. Thorneley, M. Acosta, M. B. Arnao, *J. Biol. Chem.* 1997, **272**, 5469. b) I. Schlichting, J. Berendzen, K. Chu, A. M. Stock, S. A. Maves, D. E. Benson, R. M. Sweet, D. Ringe, G. A. Petsko, S. G. Sligar, *Science*, 2000, **287**, 1615. c) P. Anzenbacher, E. Anzenbacherova, *Proc. Indian Natn. Sci. Acad.* 2003, **B69**, 883. d) N. C. Veitch, *Phytochemistry* 2004, **65**, 249. e) « Cytochrome P450 : Structure, Mechanism, and Biochemistry », ed. P. R. Ortiz de Montellano, Kluwer Academic / Plenum, 2005. f) C. Jakopitsch, J. Vlasits, B. Wiseman, P. C. Loewen, C. Obinger, *Biochemistry* 2007, **46**, 1183. g) J. Rittle, M. T. Green, *Science* 2010, **330**, 933.

5 a) Y. Shimazaki, F. Tani, K. Fukui, Y. Naruta, O. Yamauchi, *J. Am. Chem. Soc.* 2003, **125**, 10512. b) K. Asami, K. Tsukidate, S. Iwatsuki, F. Tani, S. Karasawa, L. Chiang, T. Storr, F. Thomas, Y. Shimazaki, *Inorg. Chem.* 2012, **51**, 12450. c) K. Asami, A. Takashina, M. Kobayashi, S. Iwatsuki, T. Yajima, A. Kochem, M. van Gastel, F. Tani, T. Kohzuma, F. Thomas, Y. Shimazaki, *Dalton Trans.* 2014, **43**, 2283.

6 F. Thomas, O. Jarjayes, C. Duboc, C. Philouze, E. Saint-Aman, J. L. Pierre, *Dalton Trans.* 2004, 2662. b) M. Orio, O. Jarjayes, H. Kanso, C. Philouze, F. Neese, F. Thomas, *Angew. Chem. Int. Ed.* 2010, **49**, 4989. c) A. Kochem, O. Jarjayes, B. Baptiste, C. Philouze, H. Vezin, K. Tsukidate, F. Tani, M. Orio, Y. Shimazaki, F. Thomas, *Chem.–Eur. J.* 2012, **18**, 1068.

7 a) Y. Wang, T. D. P. Stack, *J. Am. Chem. Soc.* 1996, **118**, 13097. b) Y. Wang, J. L. Dubois, B. Hedman, K. O. Hodgson, T. D. P. Stack, *Science* 1998, **279**, 537. c) R. C. Pratt, T. D. P. Stack, *J. Am. Chem. Soc.* 2003, **125**, 8716. d) R. C. Pratt, T. D. P. Stack, *Inorg. Chem.* 2005, **44**, 2367. e) T. Storr, P. Verma, R. C. Pratt, E. C. Wasinger, Y. Shimazaki, T. D. P. Stack, *J. Am. Chem. Soc.* 2008, **130**, 15448. f) P. Verma, R. C. Pratt, T. Storr, E. C. Wasinger, T. D. P. Stack, *Proc. Nat. Acad. Sci. U.S.A.* 2011, **108**, 18600. g) R. C. Pratt, C. T. Lyons, E. C. Wasinger, T. D. P. Stack, *J. Am. Chem. Soc.* 2012, **134**, 7367.

8 M. W. Bouwkamp, A. C. Bowman, E. Lobkowsky, P. J. Chirik, *J. Am. Chem. Soc.* 2006, **128**, 13340. S. K. Russell, E. Lobkowsky, P. J. Chirik, *J. Am. Chem. Soc.* 2011, **133**, 8858.

9 A. I. Nguyen, R. A. Zarkesh, D. C. Lacy, M. K. Thorson, A. F. Heyduk, *Chem. Sci.* 2011, **2**, 166.

10 C. A. Lippert, S. A. Arnstein, C. D. Sherrill, J. D. Soper, *J. Am. Chem. Soc.* 2010, **132**, 3879. A. L. Smith, K. I. Hardcastle, J. D. Soper, *J. Am. Chem. Soc.* 2010, **132**, 14358.

11 K. J. Blackmore, N. Lal, J. W. Ziller, A. F. Heyduk, *J. Am. Chem. Soc.* 2008, **130**, 2728. A. F. Heyduk, R. A. Zarkesh, A. I. Nguyen, *Inorg. Chem.* 2011, **50**, 9849.

12 a) Z. Xiao, P. S. Donnelly, M. Zimmermann, A. G. Wedd, *Inorg. Chem.* 2008, **47**, 4338. b) B. M. Paterson, J. A. Karas, D. B. Scanlon, J. M. White, P. S. Donnelly, *Inorg. Chem*. 2010, **49**, 1884.

13 a) A. R. Cowley, J. R. Dilworth, P. S. Donnelly, E. Labisbal, A. Sousa, *J. Am. Chem. Soc.* 2002, **124**, 5270. b) S. Lhuachan, S. Siripaisarnpipat, N. Chaichit, *Eur. J. Inorg. Chem.* 2003, 263. c) L. J. Ashfield, A. R. Cowley, J. R. Dilworth, P. S. Donnelly, *Inorg. Chem.* 2004, **43**, 4121. d) L. Alsop, A. R. Cowley, J. R. Dilworth, P. S. Donnelly, J. M. Peach, J. T. Rider, *Inorg. Chim. Acta* 2005, **358**, 2770. e) A. R. Cowley, J. R. Dilworth, P. S. Donnelly, J. M. White, *Inorg. Chem.* 2006, **45**, 496.

14 a) R. I. Maurer, P. J. Blower, J. R. Dilworth, C. A. Reynolds, Y. Zheng, G. E. D. Mullen, *J. Med. Chem.* 2002, **45**, 1420. b) J. P. Holland, J. C. Green, J. R. Dilworth, *Dalton Trans.* 2006, 783. c) J. P. Holland, F. I. Aigbirhio, H. M. Betts, P. D. Bonnitcha, P. Burke, M. Christlieb, M. G. C. Churchill, A. R. Cowley, J. R. Dilworth, P. S. Donnelly, J. C. Green, J. M. Peach, S. R. Vasudevan, J. E. Warren *Inorg. Chem*. 2007, **46**, 465. d) J. P. Holland, P. J. Barnard, D. Collison, J. R. Dilworth, R. Edge, J. C. Green, J. M. Heslop, E. J. L. McInnes, C. G. Salzmann, A. L. Thompson, *Eur. J. Inorg. Chem.* 2008, 3549. e) B. M. Paterson, J. A. Karas, D. B. Scanlon, J. M. White, P. S. Donnelly, *Inorg. Chem*. 2010, **49**, 1884.

15 a) C. R. Kowol, E. Reisner, I. Chiorescu, V. B. Arion, M. Galanski, D. V. Deubel, B. K. Keppler, *Inorg. Chem.* 2008, **47**, 11032. b) C. R. Kowol, R. Trondl, P. Heffeter, V. B. Arion, M. A. Jakupec, A. Roller, M. Galanski, W. Berger, B. K. Keppler, *J. Med. Chem.* 2009, **52**, 5032.

16 Y. A. Simonov, L. P. Battaglia, A. B. Corradi, G. Pelosi, M. D. Revenco, N. V. Gerbeleu, *Acta Crystallogr.* 1991, ***C47***, 1826.

17 a) S. Blanchard, F. Neese, T. Weyhermüller, K. Wieghardt, *Inorg. Chem.* 2004, **43**, 2324. b) S. Blanchard, F. Neese, E. Bothe, E. Bill, T. Weyhermüller, K. Wieghardt, *Inorg. Chem.* 2005, **44**, 3636.

18 M. A. Ali, P. V. Bernhardt, M. A. H. Brax, J. England, A. J. Farlow, G. R. Hanson, L. L. Yeng, A. H. Mirza, K. Wieghardt, *Inorg. Chem.* 2013, **52**, 1650.

19 a) S. Lhuachan, S. Siripaisarnpipat, N. Chaichit, *Eur. J. Inorg. Chem.* 2003, 263. b) C E. Labisbal, K. D. Haslow, A. Sousa-Pedrares, J. Valdes-Martinez, S. Hernandez-Ortega and D. X. West, *Polyhedron*,

2003, **22**, 2831. c) A. Castineiras, M. Gil, E. Bermejo and D. X. West, *Polyhedron*, 2001, 20, 449. d) R. Prabhakaran, R. Karvembu, T. Hashimoto, K. Shimizu and K. Natarjan, *Inorg. Chim. Acta* 2005, **358**, 2093. e) G. E. de Sousa, L. C. C. Manso, E. S. Lang, C. C. Gatto and B. Mahie, *J. Mol. Struct.* 2007, **826**, 185. f) V. V. Bon, S. I. Orysyk, V. L. Pekhuyo and S. V. Volkov, J. Mol. Struct., 2010, 984, 15. g) T. S. Lobana, P. Kumari, G. Hundal, R. J. Butcher, *Polyhedron*, 2010, **29**, 1130. h) Y.-T. Wang, H.-L. Li, J.-G. Wang, *Z. Kristallogr.–New Cryst. Struct*. 2010, **225**, 79. i) M. Cindric, M. Uzelac, D. Cincic, I. Halasz, G. Pavlovic, T. Hrenar, M. Curic, D. Kovcevic, *CrystEngComm.* 2012, **14**, 3039.

20 a) V. B. Arion, P. Rapta, J. Tesler, S. S. Shova, M. Breza, K. Luspai, J. Kozisek, *Inorg. Chem.* 2011, **50**, 2918. b) V. B. Arion, S. Platzer, P. Rapta, P. Machata, M. Breza, D. Vegh, L. Dunsch, J. Tesler, S. Shova, T. C. O. Mac Leod, A. J. L. Pombeiro, *Inorg. Chem.* 2013, **52**, 7524.

21 a) E. Lopez-Torres, M. A. Mendiola, C. J. Pastor, B. Souto Perez, *Inorg. Chem.* 2004, **43**, 5222. b) P. J. Blower, T. C. Castle, A. R. Cowley, J. R. Dilworth, P. S. Donnelly, E. Labisbal, F. E. Sowrey, S. J. Teat, M. J. Went, *Dalton Trans.* 2003, 4416.

22 K. S. Min, T. Weyhermüller, E. Bothe, K. Wieghardt, *Inorg. Chem.* 2004, **43**, 2922.

23 a) O. Rotthaus, O. Jarjayes, F. Thomas, C. Philouze, C. Perez Del Valle, E. Saint-Aman, J. L. Pierre, *Chem.–Eur. J.* 2006, **12**, 2293. b) O. Rotthaus, F. Thomas, O. Jarjayes, C. Philouze, E. Saint-Aman, J. L. Pierre, *Chem.–Eur. J.* 2006, **12**, 6953. c) O. Rotthaus, O. Jarjayes, C. Perez del Valle, C. Philouze, F. Thomas, *Chem. Commun.* 2007, 4462. d) T. Storr, E. C. Wasinger, R. C. Pratt, T. D. P. Stack, *Angew. Chem. Int. Ed.* 2007, **46**, 5198. e) L. Benisvy, R. Kannapan, Y. Song, S. Milikisyants, M. Huber, I. Mutikainen, U. Turpeinen, P. Gamez, L. Bernasconi, E. J. Baerends, F. Hartl, J. Reedijk, *Eur. J. Inorg. Chem.* 2007, 637. f) Y. Shimazaki, T. D. P. Stack, T. Storr, T. *Inorg. Chem.* 2009, **48**, 8383. g) O. Rotthaus, O. Jarjayes, C. Philouze, C. Perez Del Valle, F. Thomas, *Dalton Trans.* 2009, 1792. h) A. Kochem, M. Orio, O. Jarjayes, F. Neese, F. Thomas, *Chem. Commun.* 2010, **46**, 6765. i) M. Orio, O. Jarjayes, H. Kanso, C. Philouze, F. Neese, F. Thomas, *Angew. Chem. Int. Ed.* 2010, **49**, 4989. j) T. Storr, P. Verma, Y. Shimazaki, E. C. Wasinger, T. D. P. Stack, *Chem.–Eur. J.* 2010, **16**, 8980. k) Y. Shimazaki, N. Arai, T. J. Dunn, T. Yajima, F. Tani, C. F. Ramogida, T. Storr, *Dalton Trans.* 2011, **40**, 2469. l) L. Chiang, A. Kochem, O. Jarjayes, T. J. Dunn, H. Vezin, M. Sakaguchi, T. Ogura, M. Orio, Y. Shimazaki, F. Thomas, T. Storr, *Chem.–Eur. J.* 2012, **18**, 14117. m) A. Kochem, L. Chiang, B. Baptiste, C. Philouze, N. Leconte, O. Jarjayes, T. Storr, F. Thomas, *Chem.–Eur. J.* 2012, **18**, 14590. n) D. de Bellefeuille, M. S. Askari, B. Lassalle-Kaiser, Y. Journaux, A. Aukauloo, M. Orio, F. Thomas, X. Ottenwaelder, *Inorg. Chem.* 2012, **51**, 12796.

24 a) D. Herebian, P. Ghosh, H. Chun, E. Bothe, T. Weyhermüller, K. Wieghardt, *Eur. J. Inorg. Chem.* 2002, 1957. b) X. Sun, H. Chun, K. Hildenbrand, E. Bothe, T. Weyhermüller, F. Neese, K. Wieghardt, *Inorg. Chem.* 2002, **41**, 4295.

25 a) W. Rundel, *Chem. Ber.* 1969, **102**, 359. b) S. Kimura, E. Bill, E. Bothe, T. Weyhermu1ller, K. Wieghardt *J. Am. Chem. Soc.* 2001**,** **123**, 6025.

26 K. S. Min, T. Weyhermüller, K. Wieghardt, *Dalton Trans.* 2003, 1126.

27 C. C. Lu, E. Bill, T. Weyhermüller, E. Bothe, K. Wieghardt, *J. Am. Chem. Soc.* 2008, **130**, 3181.

28 M. Valente, C. Freire, B. de Castro, *J. Chem. Soc., Dalton Trans.* 1998, 1557.

29 V. V. Saraev, P. B. Kraikivskii, P. G. Lazarev, G. Myagmarsuren, V. S. Tkach, F. K. Schmidt, *Russ. J. Coord. Chem.* 1996, **22**, 615.

30 M. J. Page, W. Y. Lu, R. C. Poulten, E. Carter, A. G. Algarra, B. M. Kariuki, S. A. Macgregor, M. F. Mahon, K. J. Cavell, D. M. Murphy, M. K. Whittlesey, *Chem. Eur. J.* 2013, **19**, 2158.

31 R. S. Drago, E. I. Baucom, *Inorg. Chem.* 1972, **11**, 2064. F.V. Lovecchio, E. S. Gore, D. H. Busch, *J. Am. Chem. Soc.* 1974, **96**, 3109. H. J. Krüger, R. H. Holm, *Inorg. Chem.* 1987, **26**, 3645. P. A. Connick, K. A. Macor, *Inorg. Chem.* 1991, **10**, 4654. T. J. Collins, T. R. Nichols, E. S. Uffelman, *J. Am. Chem. Soc.* 1991, **113**, 4708. F. Azevedo, M. A. Carrondo, B. Castro, M. Convery, D. Domingues, C. Freire, M. T. Duarte, K. Nielsen, I. C. Santos, *Inorg. Chim. Acta* 1994, **219**, 43. D. Pinho, P. Gomes, C. Freire, B. De Castro, *Eur. J. Inorg. Chem.* 2001, 1483. Z. Xiao, B.O. Patrick, D. Dolphin, *Inorg. Chem.* 2003, **42**, 8125.

32 a) M. Kolberg, G. Bleifuss, A. Gräslund, B.-M. Sjöberg, W. Lubitz, F. Lendzian, G. Lassmann, *Arch. Biochem. Biophys.* 2002, **403**, 141. b) G. Lassmann, M. Kolberg, G. Bleifuss, A. Gräslund, B.-M. Sjöberg, W. Lubitz, *Phys. Chem. Chem. Phys.* 2003, **5**, 2442. b) M. van Gastel, W. Lubitz, G. Lassmann, F. Neese, *J. Am. Chem. Soc.* 2004, **126**, 2237.

33 K. Ray, T. Petrenko, K. Wieghardt, F. Neese, *Dalton Trans.* 2007, 1552.

34 C. Adamo, R. Subra, A. Di Matteo, V. Barone, *J. Chem. Phys.* 1998, **109**, 10244.

35 SADABS, Bruker–Siemens Area Detector Absorption and Other Correction, G.M. Sheldrick, University of Göttingen, Germany, 2006, Version 2008/1.

36 O. V. Dolomanov, L. J. Bourhis, R. J. Gildea, J. A. K. Howard, H. Puschmann, *J. Appl. Cryst.* 2009, **42**, 339.

37 F. Neese, ORCA «an ab initio, Density Functional and Semiempirical Program Package », version 3.0.0; Max Planck Institute for Chemical Energy Conversion: Mülheim, Germany, 2013. F. Neese, Wiley *Interdiscip. Rev. Comput. Mol. Sci.* 2012, **2**, 73.

38 J. P. Perdew, *Phys. Rev. B* 1986, **33**, 8822.

39 J. P. Perdew, *Phys. Rev. B* 1986, **34**, 7406.

40 A. D. Becke, *Phys. Rev. A* 1988, **38**, 3098.

41 A. Schäfer, C. Huber, R. Ahlrichs, *J. Chem. Phys.* 1994, **100**, 5829.

42 F. Neese, *J. Comput. Chem.* 2003, **24**, 1740.

43 F. Weigend, *Phys. Chem. Chem. Phys.* 2006, **8**, 1057.

44 A. Klamt, G. Schürmann, *J. Chem. Soc., Perkin Trans. 2* 1993, 799.

45 A. D. Becke, *J. Chem. Phys.* 1993, **98**, 1372.

46 C. T. Lee, W. T. Yang, R. G. Parr, *Phys. Rev. B* 1988, **37**, 785.

47 M. E. Casida, in *Recent Advances in Density Functional Methods*, Chong, D.P. Ed. World Scientific: Singapore, 1995.

48 S. Hirata, M. Head-Gordon, *Chem. Phys. Lett.* 1999, **314**, 291.

49 S. Hirata, M. Head-Gordon, *Chem. Phys. Lett.* 1999, **302**, 375.

50 F. Neese, G. Olbrich, *Chem. Phys. Lett.* 2002, **362**, 170.

51 J. Vinsova, K. Cermakova, A. Tomeckova, M. Ceckova, J. Jampilek, P. Cermak, J. Kunes, M. Dolezale, F. Staud, *Bioorg. Med. Chem.* 2006, **14**, 5850.

52 S. Y. Shaban, M. M. Ibrahim, F. W. Heinemann, *Inorg. Chim. Acta.* 2007, **360**, 2929.

.

Table of Content

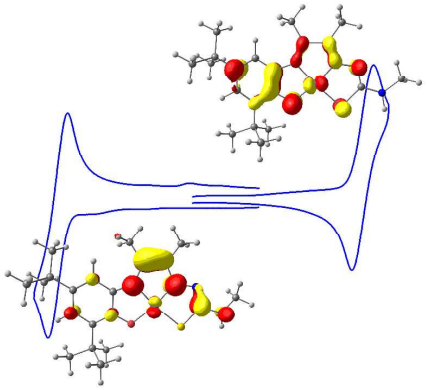

The neutral nickel(II) complexes are chameleon pro-radical compounds: Under their one-electron oxidized form they feature an iminosemiquinonate (or iminothiosemiquinonate) radical, while under their reduced form they are α-diimine π-radicals.